

Article

Improving Structural Safety of L-Type Flange Joint for Wind Towers

Thanh-Tuan Tran ^{1,2}, Sangkyun Kang ³ and Daeyong Lee ^{1,*}

¹ Institute of Offshore Wind Energy, Kunsan National University, 558 Daehak-ro, Gunsan 54150, Jeollabuk-do, Republic of Korea

² Advanced Structural Engineering Laboratory, Department of Structural Engineering, Faculty of Civil Engineering, Ho Chi Minh City Open University, Ho Chi Minh City 700000, Vietnam

³ Department of Mechanical Engineering, Kunsan National University, 558 Daehak-ro, Gunsan 54150, Jeollabuk-do, Republic of Korea

* Correspondence: daeyong.lee@kunsan.ac.kr; Tel.: +82-10-4490-0980

Abstract: This paper focuses on the design modification of L-type flange joint geometry in wind towers, aiming to enhance its structural safety. For this aim, current design issues of existing flange joints are discussed. The numerical simulations indicate that the threaded bolt and flange-to-shell junction are critical locations where failure may happen. Further discussion to improve structural safety is applied for an existing 5 MW flange joint. Through parametric studies, the major factors influencing ultimate strength are identified. The results show that the aspect ratio plays an important role in increasing the structural safety of the flange joints, while the width of the flange segment weakens the stiffness of the flange-to-shell junction. The findings in this study are expected to provide a useful reference for designing the L-type flange joints in practical engineering fields.

Keywords: wind tower; L-type flange joint; failure mode; finite element modeling

Citation: Tran, T.-T.; Kang, S.; Lee, D. Improving Structural Safety of L-type Flange Joint for Wind Towers. *Energies* **2022**, *15*, 8967. <https://doi.org/10.3390/en15238967>

Academic Editor: José António Correia

Received: 18 October 2022

Accepted: 23 November 2022

Published: 27 November 2022

Publisher's Note: MDPI stays neutral with regard to jurisdictional claims in published maps and institutional affiliations.



Copyright: © 2022 by the authors. Licensee MDPI, Basel, Switzerland. This article is an open access article distributed under the terms and conditions of the Creative Commons Attribution (CC BY) license (<https://creativecommons.org/licenses/by/4.0/>).

1. Introduction

According to the track records of wind turbine accidents [1], the collapse of the steel tower is one of the critical modes in wind turbines [2–5]. This failure is caused by different reasons, such as buckling failure due to the instability of the tower tubes [6–8] and failure of the flange joints [9–13], etc. The failure of the flange joints has been studied as an important mechanism related to the collapse of wind structures (see Figure 1) [10,14–17].

Regarding the collapse of the flange joints, the ultimate resistance is a significant factor as it represents the load-carrying capacity of the joint. There are a variety of parameters that impact the ultimate resistance, including bolt pretension load [18], skew effect [11], flange geometry [19], and number of bolts, etc. The challenge is how to consider these factors to improve structural safety when designing the flange joints.

Initial analytical models to calculate the ultimate resistance of the flange joints were developed by Petersen [20]. With this work, Petersen developed different failure mechanisms for L-type flange joints, including mode A (bolt failure), mode B (bolt failure and plastic hinge in flange-to-shell junction), and mode C (plastic hinge in the flange and flange-to-shell junction). Later, several modifications were been studied by Seidel [21] and Tobinaga and Ishihara [22], considering the influence of prying forces.

Moreover, numerical simulations are attracting the attention of many researchers. Seidel et al. [11] evaluated the influence of geometrical imperfections on the load-bearing behavior of the flange joint via numerical and experimental simulations. Ślęczka and Leń [19] investigated the effects of structural geometry on the performance of flange joints using finite element analysis (FEA). With this work, Ślęczka and Leń found that, when increasing diameters, the restraining effects of the circular shape of the flange and tube

wall decrease. Additionally, the bolt pretension load significantly affects the additional bolt force and fatigue life of the flange joints, as stated in the works by Okorn et al. [18].

Despite resolving the fundamental issues related to the effects of geometrical parameters on the load-carry capacity, previous literature has paid less attention to which part of structural geometries has the most influence. To achieve this objective, the limitations of the current design practice of the flange joint are discussed. Based on the finite element analysis, two yielding cases (i.e., yielding in bolt and yielding in flange-to-shell junction), which are known as the first yielding stages of the flange joint, are identified. Using these failure modes, targeting that the flange-to-shell junction will fail before high-strength bolts, an existing 5 MW flange joint is redesigned, aiming to improve its structural safety.



Figure 1. Failure of wind towers.

2. Numerical Simulation of the Existing Flange Joints

2.1. Finite Element Modeling

The numerical simulations are carried out for three different flange joints using the commercial software ANSYS 2021 R1. These configurations are taken from the current design of wind towers in South Korea, as shown in Figure 2. The flange joint consists of three main parts (flange member, tower shell, and bolt), which are modeled with three-dimensional elements. The geometric parameters of the flange joints are summarized in Table 1. It is noted that the bolt thread is considered to have an equivalent cross-section that equals the pitch diameter. Different contact conditions are used: (i) the friction contact with the frictional coefficient of 0.176 between two flange members, (ii) the frictionless contact between the bolt and flange hole, and (iii) the bonded contact for the rest parts (i.e., flange tower, bolt washer, and flange washer). With regards to the boundary condition, the fixed condition is assigned to the bottom tower, and frictionless support is used at the two flange sides. This support is used to prevent deformation in the horizontal direction.

Multilinear material is considered to analyze the plasticity of connections. The material model, specified by the DNVGL-RP-C208 guideline [23], is applied for the flange and tower shell (Figure 3). The material properties are listed in Table 2. The material properties are available for up to 63 mm of plate thickness, which is sufficient for the tower shell. To

determine material parameters for the thicker flange (ranging from 145 mm to 200 mm), the extrapolation technique is applied based on the available data. The elasticity modulus $E = 200$ GPa and Poisson's ratio $\nu = 0.3$ are applied for all components of flange joints. The grade 10.9 is applied for high-strength bolts, and their parameters are taken from DAST 021 [24].

Loading conditions for the analysis include two steps: (1) bolt pretensioning load and (2) tensile force at the tower flange level. The application of the bolt pretensioning load follows the regulation of Eurocode 1993-1-8-2005 [25]. The tensile force (F_s) (Figure 4) applied to the single bolt strip segment is calculated from the equivalent bending moment and equivalent axial force, and it is expressed as follows: (see Appendix A)

$$F_s = \frac{1}{n_b} \left(\frac{8M_{ed}D_o}{D_o^2 + D_i^2} - N_{ed} \right) \quad (1)$$

where D_o and D_i are the outer and inner diameters of the tower shell, respectively; M_{ed} and N_{ed} are the equivalent bending moment and equivalent axial force at the flange joint, respectively, which are taken from the design load cases (DLCs). Details of the DLCs and tensile force are listed in Table 3.

In order to verify the accuracy of the finite element approach, a prototype flange segment with the available test data is used [26]. Details of verification processes can be found in Tran and Lee [27].

Table 1. Geometry of the existing flange joints.

t_f	Bolt		Tower (mm)			Flange (mm)		
	Size	n_b	d	s	s	b_f	a	b
3 MW	M56	102	4500	34	180	230	120	93
4 MW	M72	88	4200	43	145	266.5	135	110
5 MW	M56	152	6000	36	200	210	99	93

Table 2. Material properties.

Specimen	Part	Material	Thickness [mm]	σ_{prop} [MPa]	σ_{yield} [MPa]	σ_{yield2} [MPa]	σ_u [MPa]	$\epsilon_{p,y1}$ [-]	$\epsilon_{p,y2}$ [-]	$\epsilon_{p,ult}$ [-]
3 MW	Tower	EN355	34	310.5	345.0	348.4	470.0	0.004	0.02	0.15
	Flange	EN355	180	264.7	294.4	297.5	411.0	0.004	0.02	0.15
	Bolt	10.9	-	-	900.0	-	1000.0	0.00429	0.015	0.09
4 MW	Tower	EN355	43	301.5	335.0	338.4	450.0	0.004	0.02	0.15
	Flange	EN355	145	275.3	306.1	309.3	423.2	0.004	0.02	0.15
	Bolt	10.9	-	-	900.0	-	1000.0	0.004	0.02	0.15
5 MW	Tower	EN355	36	310.5	345.0	348.4	470.0	0.004	0.02	0.15
	Flange	EN355	200	258.6	287.7	290.7	404.1	0.004	0.02	0.15
	Bolt	10.9	-	-	900.0	-	1000.0	0.004	0.02	0.15

Table 3. Tensile force at the flange joint.

Specimen	DLC	Moment [kNm]					Force [kN]				F_s (kN)
		Mx	My	Mxy	Mz	Fx	Fy	Fxy	Fz		
3 MW	Mxy	Max	-2445.4	-85,509	85,544	-1726.8	-1119.5	40.2	1120.2	-5148.6	7.52×10^2
4 MW	Mx	Max	-95,607	83,008	126,614	4110.7	1106	1450.6	1824.2	-5067.9	1.33×10^3
5 MW	Mxy	Max	183,406	-38,277	187,357	8070.5	-189.3	-2385.7	2393.2	-8436.2	8.59×10^2

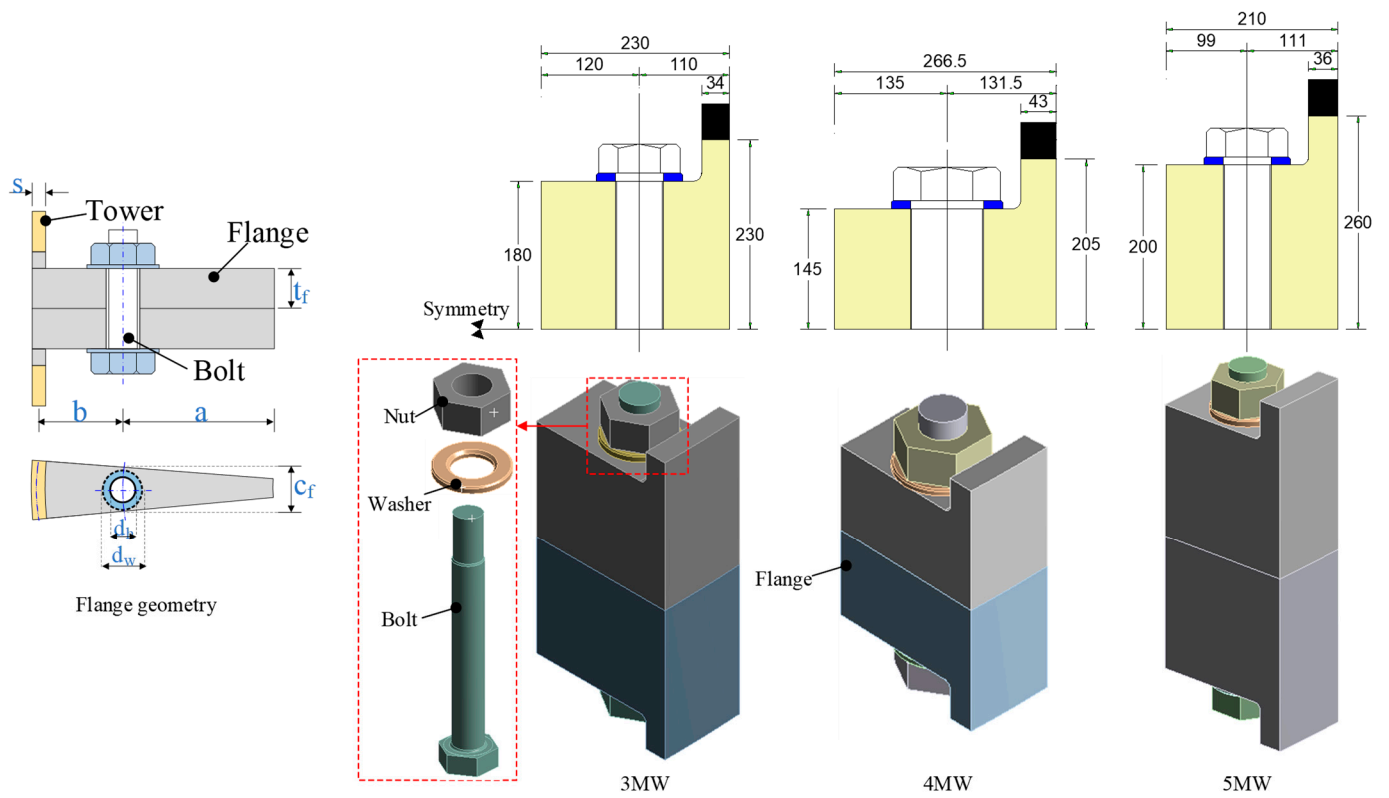


Figure 2. Geometry and corresponding finite element modeling of flange joints.

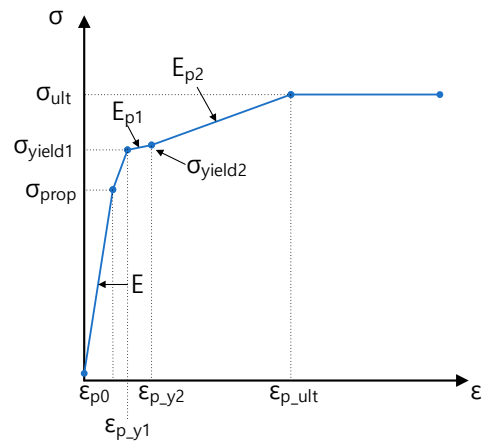


Figure 3. Stress–strain curve [23].

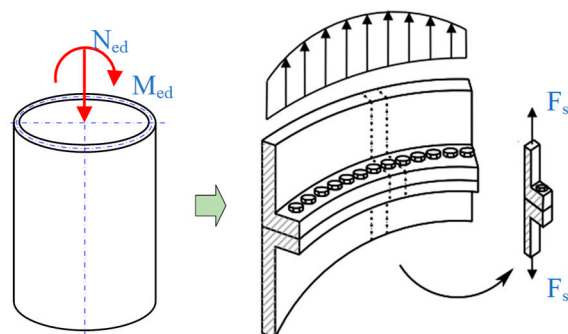


Figure 4. Tensile force applied to L-type flange segment.

2.2. Discussion on the Failure Mode of Flange Joints

The maximum axial stress and plastic strain of the flange joints under the design load are presented in Figures 5 and 6. In line with the theory, the following regions are selected due to their yield sensitivity. For the flange member, three regions (i.e., flange-to-shell junction, flange around the bolt hole, and flange inner) are investigated. In the case of the bolt member, two regions (i.e., threaded zone and head–shank transition) are considered.

Looking at Figure 5, it is found that under the design load, the stress concentrations are observed at the flange-to-shell junction. The tensile stresses of 307 MPa and 313 MPa are found for 3 MW and 4 MW, respectively. These values are higher than the yielding strength given in Table 2, leading to the yielding in the flange joints. In the case of 5 MW, the maximum tensile stress at the flange-to-shell junction is around 245 MPa, which is smaller than the yielding strength (287.7 MPa); thus, the flange member is still safe. An interesting finding is that the large zone of compressive stress occurs at the internal flange tip (with a maximum value of 395 MPa) due to the separation of the flange members. However, it is not an important region compared to the other parts due to the high thickness of the flange [28]. This can be explained as follows: in the case of flange joints, the critical failure is the result of the high tensile stress associated with the elongated material. As a result, the failure at the inner flange caused by compression can be ignored when investigating the failure locations [29].

With regards to the bolt (Figure 6), it is found that higher stresses occur on the left side of the bolt due to the bending moment. Moreover, the maximum stresses are concentrated at the (i) bolt thread and (ii) transition region between the bolt head and shank. The former location is due to its reduced diameter compared to the shank part, while the latter is caused by a sudden change in geometry. In Figure 6, the highest values of 1084 MPa and 1101 MPa are found for 3 MW and 4 MW, respectively, and they occur at the threaded zone. However, the high stresses are only found at the surface of the bolt, which is visible by creating the cross-section through the axial bolt. The relative comparison of the stress and strain distributions at the flange-to-shell junction (Figure 5) and the threaded bolt (Figure 6) shows that the threaded zone is not the cause of flange failure. In the case of 5 MW, a wide region of high stress occurs at the threaded zone, with a maximum value of 1081 MPa. This is a critical location compared to other regions leading to the failure of the bolt.

For a better understanding of the stress distribution in the flange joints, the stress linearization technique is applied. This technique is a procedure in which the stress distribution along a line through the thickness in a bolt is approximated with an equivalent linear stress distribution. In this study, the average stresses along a path of the flange and bolt members are evaluated, as shown in Figure 7. For the flange member (Figure 7.left), it is seen that the most stress occurs at the flange-to-shell junction. The values of 359 MPa and 269 MPa are found for 3 MW and 4 MW, respectively; these values are exceeding the yield strength of the flange member given in Table 2. As a result, under the design load, the flange joint fails at the flange-to-shell junction. In the case of 5 MW, the stress is below the material yield strength limit; thus, the joint is still safe.

With regards to the bolt member, it is found that the stresses are constant along the bolt shank while there is a large variation at the bolt thread (Figure 7 right). In the case of 3 MW and 4 WM, the bolts are still safe with the maximum values of 666 MPa and 394 MPa, respectively. However, the average stress for 5 MW is about 1081 MPa, which is higher than the yielding strength.

Based on the above observation, it can be concluded that the flange-to-shell junction and threaded bolt are critical locations where failure may happen. The governing failure modes of the flange joints are summarized as:

- 3 MW: failure at the flange-to-shell junction.
- 4 MW: failure at the flange-to-shell junction.
- 5 MW: failure at the threaded bolt.

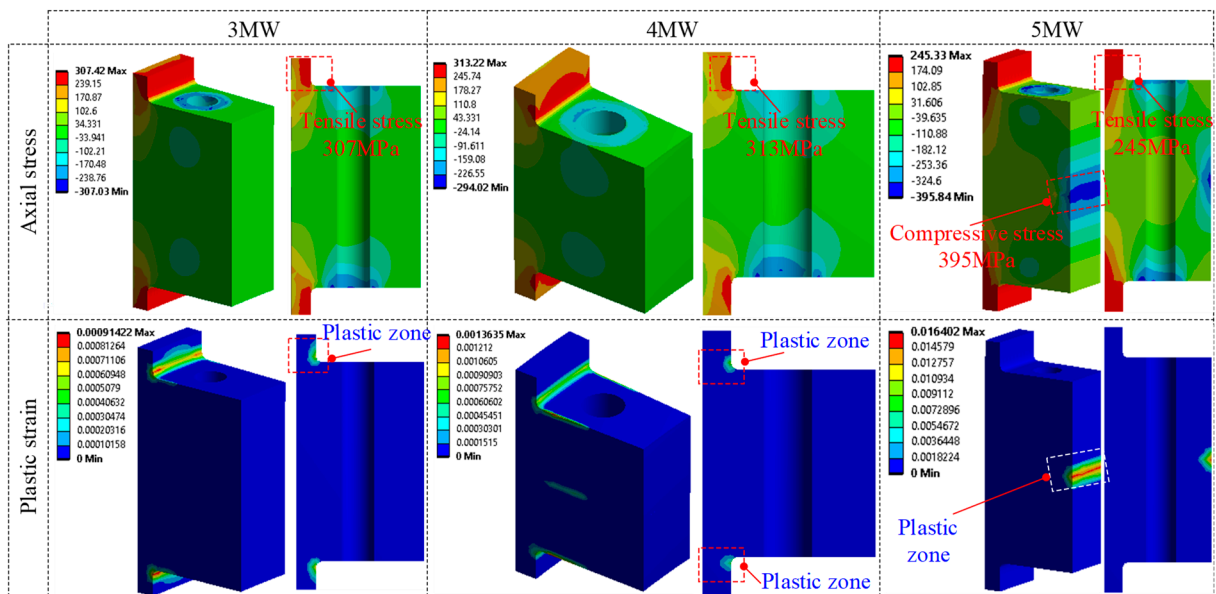


Figure 5. Axial stress and plastic strain in the flange member.

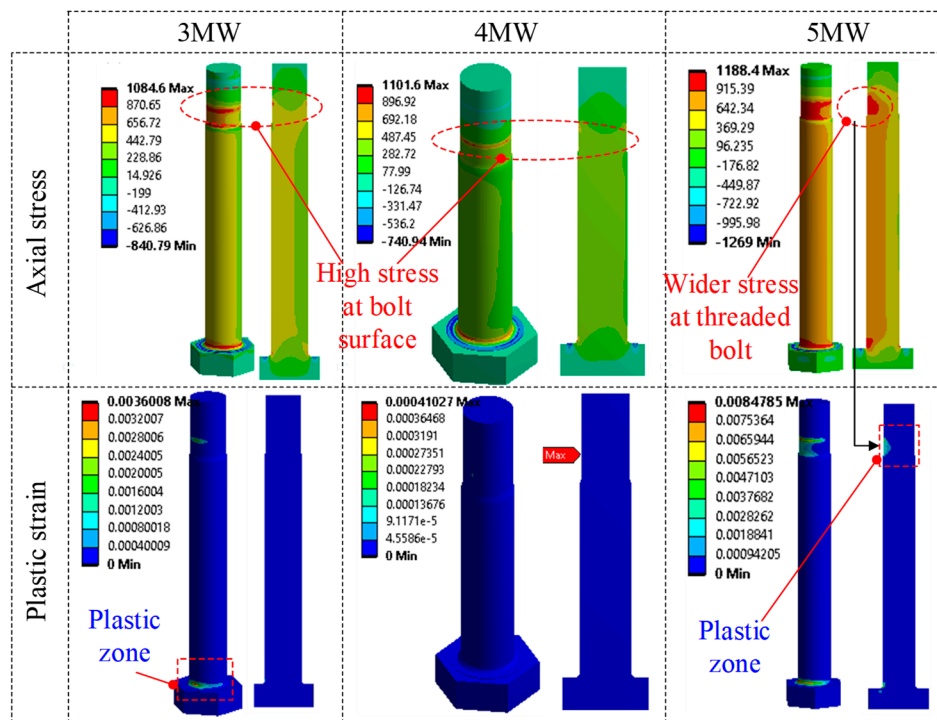


Figure 6. Axial stress and plastic strain in the bolt.

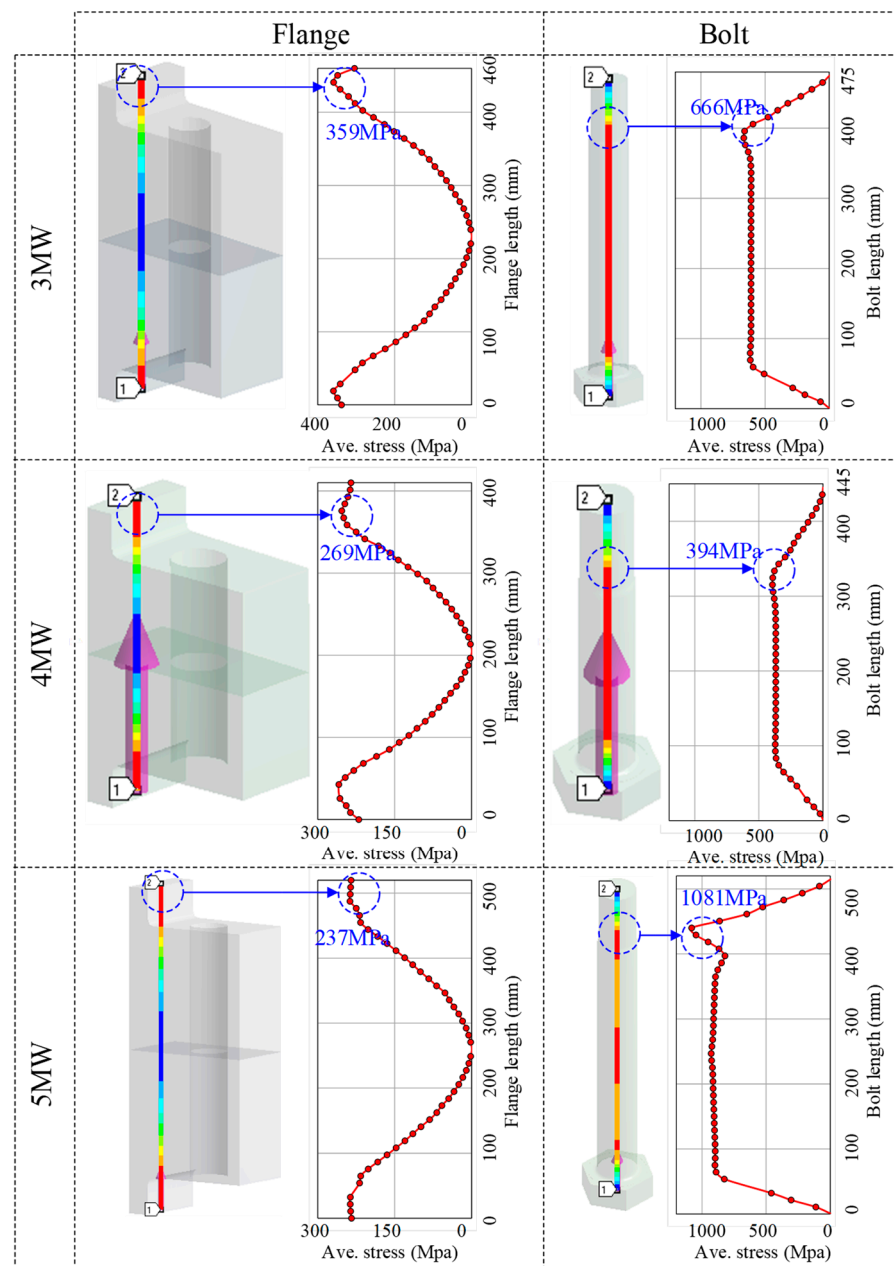


Figure 7. Global stress in the flange joints.

2.3. Limitations of the Current Design Practice

The numerical analyses show that the flange-to-shell junction and bolt thread are critical locations where the failure may happen. The failure of the bolt is brittle and more dangerous, whereas the failure of the flange-to-shell junction is ductile and foreseeable.

In this study, the 5 MW L-type flange joint will fail at the bolt member, which is not foreseeable. However, in practical engineering, it would be preferable when the flange-to-shell junction will fail before the bolt yielding. Thus, this configuration will be redesigned, aiming to improve its structural safety.

3. Redesign of the 5 MW Flange Joint

3.1. Parametric Studies

The parametric studies are performed through numerical simulations in ANSYS software. The considered geometrical parameters are listed in Table 4. The analysis cases are classified into the following groups:

- Group 0 is the original model.
- Group 1 includes models with flange thicknesses ranging from 150 to 170 mm.
- Group 2 includes models with shell thicknesses ranging from 32 to 34 mm.
- Group 3 includes models with aspect ratios ranging from 1.17 to 1.39 mm.
- Group 4 includes models with flange widths ranging from 99.42 to 139.42 mm.

To ensure the failure occurs in the flange joints, all cases are evaluated with the tensile force of 1.05 kN. The average axial stresses of the bolt and flange members are reported and compared to the original model, aiming to evaluate the efficiency of each considered variable.

Table 4. Geometrical parameters of the investigated flange joints.

Group	Tower		Bolt Size [-]	Flange						
	d [mm]	s [mm]		t_f [mm]	c_f [mm]	b_{ges} [mm]	a [mm]	b [mm]	$\omega = a/b$ [-]	
Group 0	6000	36	M56	200	119.42	210	99	93	1.06	
Group 1	6000	36	M56	170	119.42	210	99	93	1.06	
	6000	36	M56	150	119.42	210	99	93	1.06	
Group 2	6000	34	M56	200	119.42	210	100	93	1.08	
	6000	32	M56	200	119.42	210	101	93	1.09	
Group 3	6000	36	M56	200	119.42	220	109	93	1.17	
	6000	36	M56	200	119.42	230	119	93	1.28	
	6000	36	M56	200	119.42	240	129	93	1.39	
Group 4	6000	36	M56	200	109.42	210	99	93	1.06	
	6000	36	M56	200	99.42	210	99	93	1.06	
	6000	36	M56	200	129.42	210	99	93	1.06	
	6000	36	M56	200	139.42	210	99	93	1.06	

3.2. Analysis Results

3.2.1. Effect of the Flange Thickness, t_f

The influence of the flange thickness on the performance of the flange joints is shown in Figure 8. With the increase in the flange thickness, the maximum stresses that occur at the threaded bolt (bolt member) and flange-to-shell junction (flange member) are almost the same. The values of around 1100 MPa and 240 MPa are found for the bolt and flange members, respectively. The outcomes show that there has been no change in the failure mode of the flange joints; the bolt failure is still the governing one.

This observation indicates that the flange thickness has little influence on the performance of the flange joint. Thus, in practical engineering, it is significant to select a suitable thickness. The flange thickness should not be underestimated for the required value since the flange joint may be failed at the flange member. This is unexpected in the practical design of wind towers. In contrast, an overestimated thickness is meaningless since it relates to the material cost.

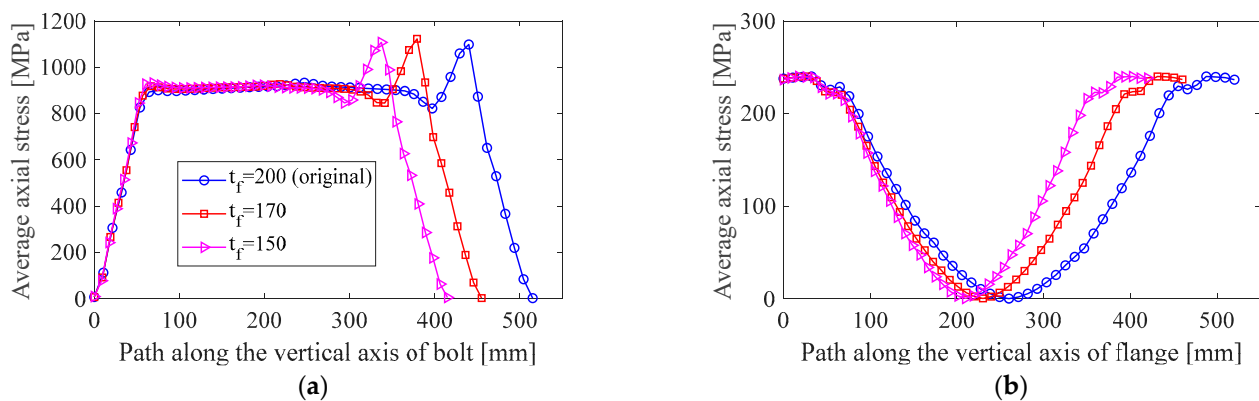


Figure 8. Influence of flange thickness on stress distributions: (a) bolt and (b) flange.

3.2.2. Effect of the Tower Thickness, s

The tower thickness has almost no effect on the stress distribution of the bolt member, the average axial stresses along the bolt with different analysis cases overlap with each other (Figure 9a), and the maximum stress is about 1100 MPa, distributed at the threaded zone. However, the stress distribution of the flange member shows an increasing tendency at the flange-to-shell junction due to the stiffness decrement (Figure 9b). Compared to the original model ($s = 36$ mm), the increments of 5.9% and 12.5% are found for $s = 34$ mm and $s = 32$ mm, respectively. It is noted that these values are below the material yield strength limit. Through relative comparison of the stress distribution between the flange and bolt members, it is shown that the failure of the threaded zone is the governing one.

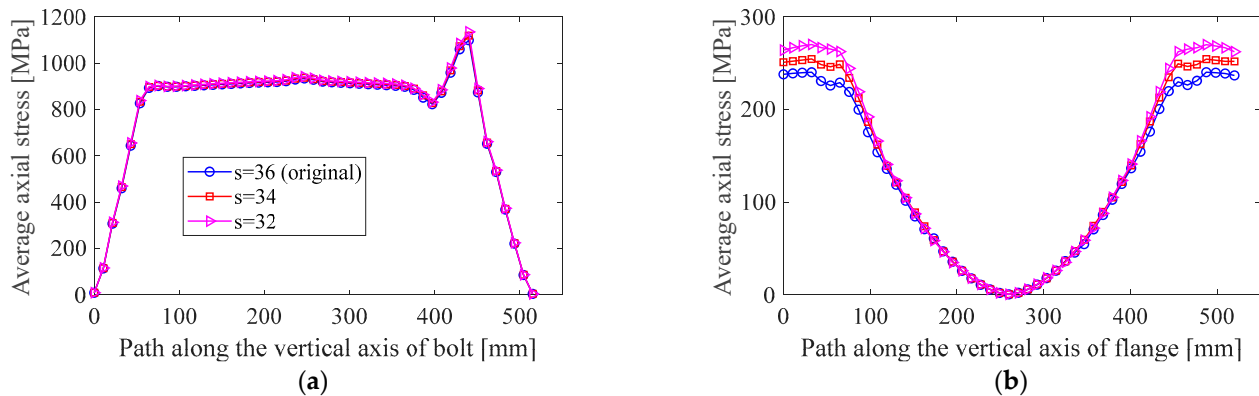


Figure 9. Influence of shell thickness on stress distributions: (a) bolt and (b) flange.

3.2.3. Effect of the Aspect Ratio, ω

In general, the influence of ratio ω on the performance of the flange member is small (Figure 10b). As ω increases, the stress distributions are almost the same each other, and the maximum value occurring at the flange-to-shell junction is around 240 MPa. However, the aspect ratio ω has a remarkable influence on the stress distribution of the bolt member (Figure 10a). As the ω increases, the stress of the bolt decreases. When the ω increases to 1.39, the maximum stress is smaller than 17.8% compared to the original model. This means that increasing the ratio ω is one of the methods to increase the structural safety of the flange joint.

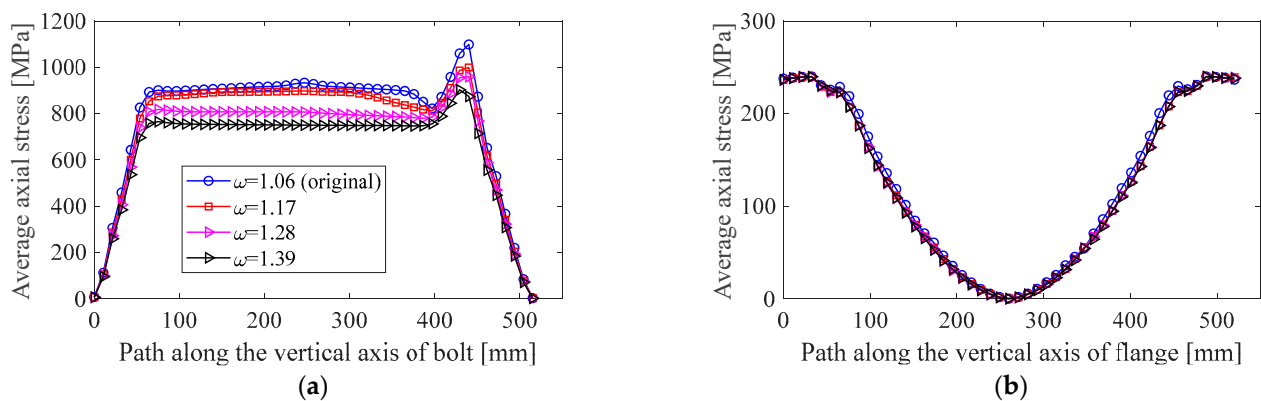


Figure 10. Influence of aspect ratio on stress distributions: (a) bolt and (b) flange.

3.2.4. Effect of the Flange Width, c_f

The flange width has little effect on the performance of the bolt member of the flange joint (Figure 11a). An interesting finding is that decreasing the flange width is the cause of higher stress in the middle bolt. When c_f is reduced to 99.42 mm, an increment of 6.3% can be found compared to group 0. It is noted that this effect can be reduced by applying the bolt preload in practical engineering. In contrast, the flange width has a great effect on the performance of the flange member (Figure 11b). When c_f is reduced to 99.42 mm, the maximum stress increases up to 335.8 MPa, leading to the failure at the flange-to-shell junction. Therefore, reducing the flange width is the way to control the failure at the flange joint.

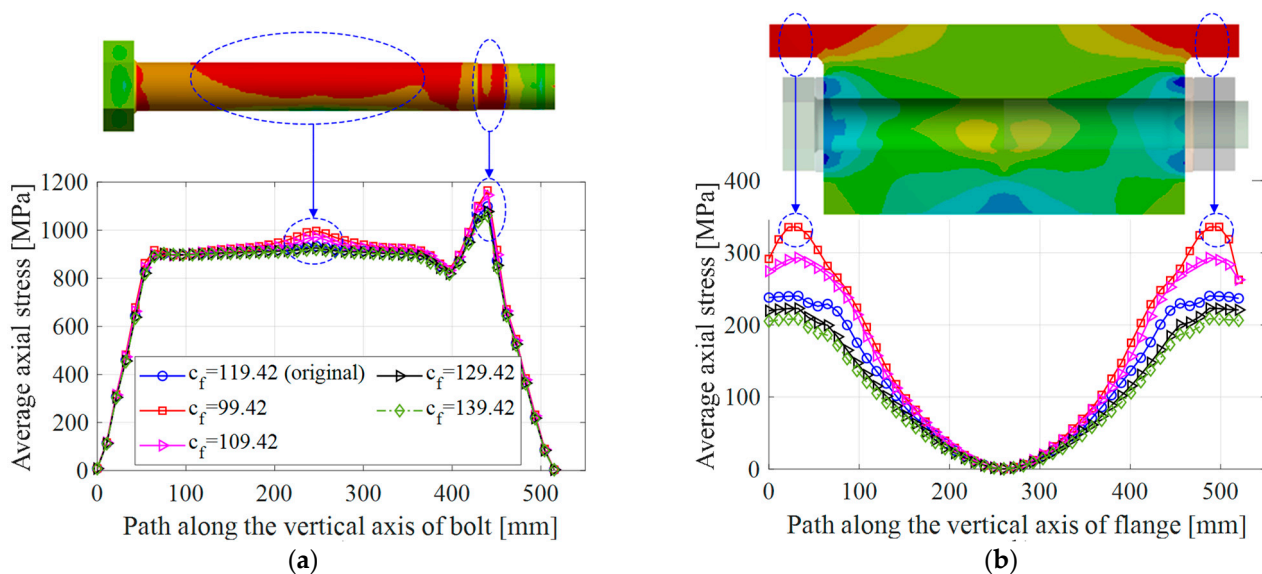


Figure 11. Influence of flange width on stress distributions: (a) bolt and (b) flange.

3.3. New Design of the Existing 5 MW Flange Joint

Based on the outcomes from the parametric analysis, to obtain the failure at the flange-to-shell junction, the following points should be noted:

1. Decrease the flange width (c_f): this aims to control the failure at the flange joint.
2. Increase the aspect ratio (ω): this aims to increase the safety of the bolt member and reduce the compressive stress at the inner flange–flange.
3. Moreover, the flange thickness (s) can be decreased to save material costs.

From the above statements, a new design of the existing 5 MW flange joint is recommended. The structural parameters are summarized in Table 5. A comparison of stress

distributions in the bolt and flange members under the design load (DLC = 859.5 kN) is given in Figure 12.

In general, the new design has the best performance compared to the current configuration. For the flange member (Figure 12b), locations of the stress concentration are found to be the same as each other (at the flange-to-shell junction). However, the new design has higher stress than the existing configuration, with a difference of 27.5%. With regards to the bolt member (Figure 12a), the results indicate that the stress of the new configuration is smaller than the existing design, with a difference of about 22%. The location of stress concentration is found at the threaded zone, with the values of 783 MPa and 609 MPa for the new design and existing configuration, respectively. Additionally, the resultant force in the bolt is evaluated (Figure 13). The value of 1690.6 kN is found for the current design, which is higher than the yielding force of the bolt (1462 kN). While the new design, with a value of 1374.3 kN, is below the yielding force limit, it satisfies the ultimate criteria. Based on the relative comparison of stress distribution in the flange and bolt members, it can be concluded that the new design tends to be failed at the flange-to-shell junction.

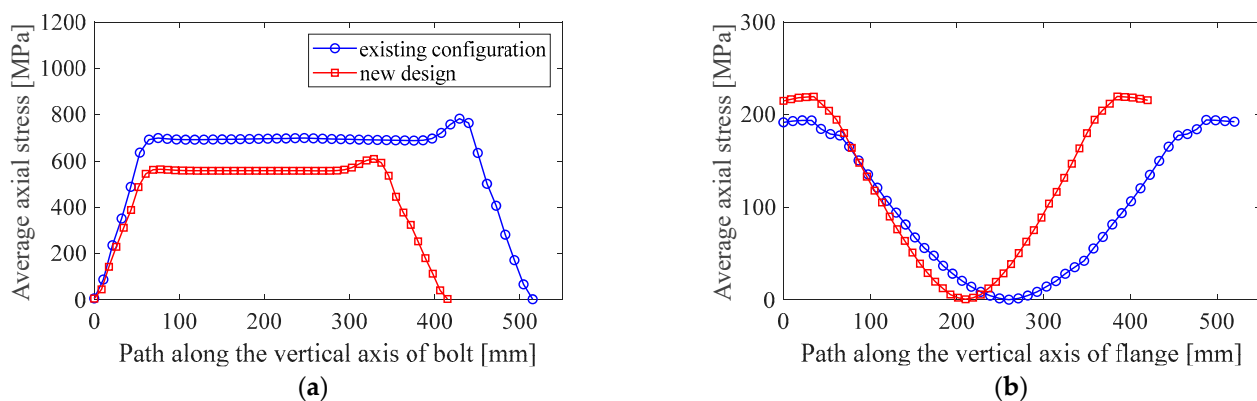


Figure 12. Stress distribution under design load: (a) bolt and (b) flange.

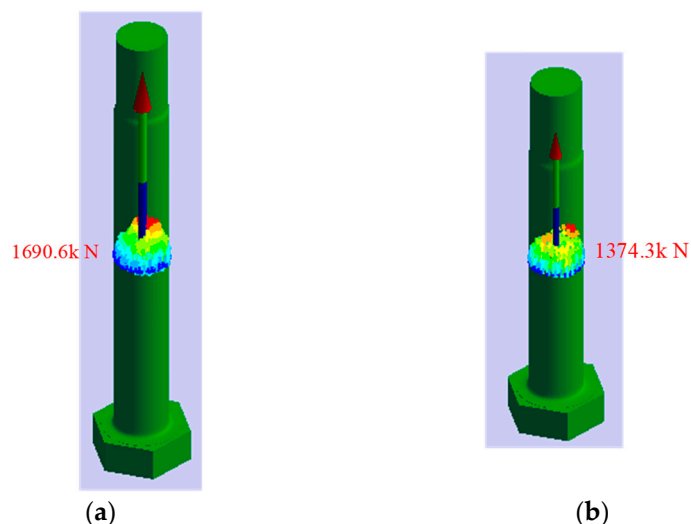


Figure 13. Resultant force of bolt: (a) existing configuration and (b) new design.

To better see the failure mode in the flange joint, increasing the tensile load up to 1050 kN at the tower shell is considered. Similar observations are made for the stress distribution of bolt and flange members, as shown in Figure 14. With regards to the bolt member, high stress is concentrated at the bolt thread, with the average values of up to 1081 MPa and 940 MPa for the existing configuration and new design, respectively. It is

noted that a wider yield region at the existing configuration is found compared to the new design. In the case of the flange member, the high-stress concentrations are at the flange-to-shell junction, with the maximum values of 237 MPa and 302 MPa for the existing configuration and new design, respectively. It is noted that in the new configuration, a larger yield region occurs at the threaded zone compared to the existing design. A comparison between the bolt and flange shows that the flange joint will be failed at the flange-to-shell junction, which can be seen through the illustration of the plastic strain (Figure 15).

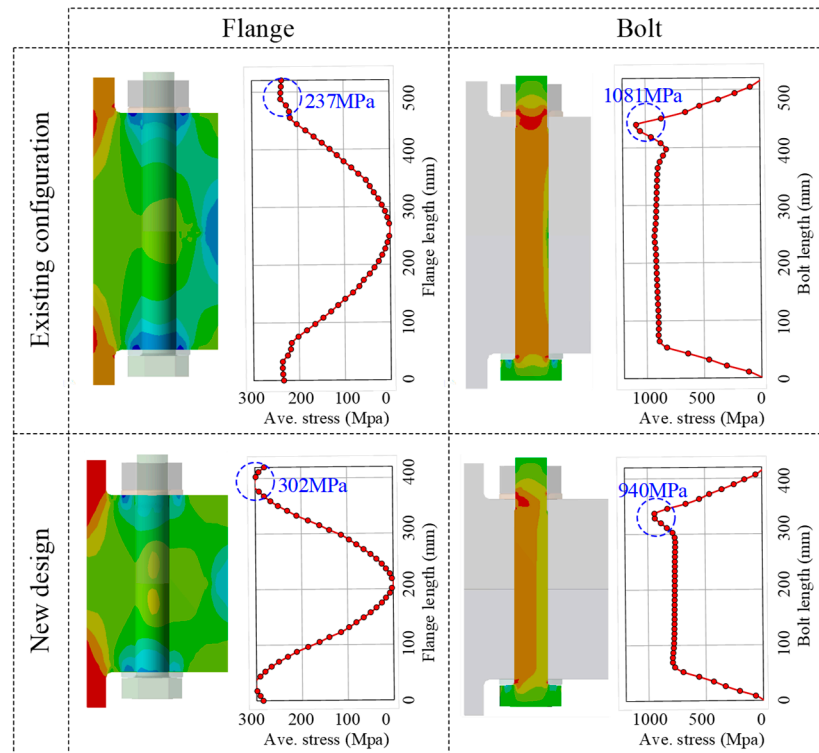


Figure 14. Stress distribution under $F_s = 050$ kN.

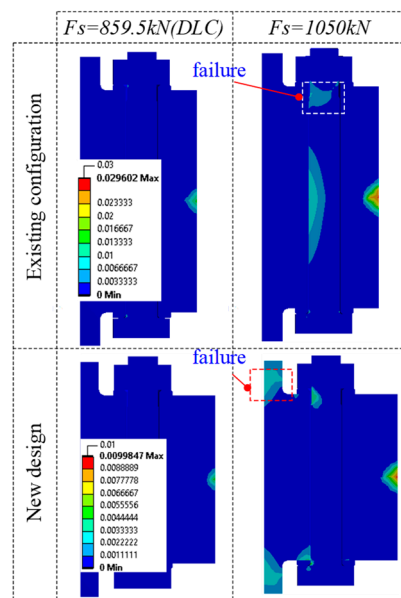


Figure 15. Failure of flange joint.

Furthermore, the mass and number of bolts are also compared, as shown in Table 5. The results show that the total weight of the new design is about 14.5% smaller than that

of the existing configuration. However, an additional total of 14 bolts is required for the new concept.

Table 5. Comparison of existing configuration and new design.

Model	Geometry						Weight <i>m</i> [T]	Number of Bolts <i>n_b</i> [-]	
	Tower		Flange						
	<i>d</i> [mm]	<i>s</i> [mm]	<i>t_f</i> [mm]	<i>c_f</i> [mm]	<i>b_{ges}</i> [mm]	<i>a</i> [mm]			<i>b</i> [mm]
Existing configuration	6000	36	200	119.42	210	99	93	6.315	152
New design	6000	32	150	99.42	240	131	93	5.396	166

4. Conclusions

The present work aims to provide a thorough understanding of the behavior of the L-type flange joint in the wind turbine tower and a new design approach for this connection. The main conclusions are listed as follows:

- Numerical simulation is an effective way to simulate various failure modes of the flange joints. The observed outcomes indicate that threaded bolt and flange-to-shell junction are the critical locations, leading to the failure in the flange joint.
- Following the parametric studies, it is found that the aspect ratio ω plays an important role in increasing the structural safety of the flange joint. The width of the flange segment will weaken the stiffness of the flange-to-shell junction. These parameters are useful in controlling the failure mode of the flange joint. Additionally, the flange and tower thicknesses have small influences on the performance of the connection.
- A design modification of an existing 5 MW flange joint is carried out to enhance its structural safety. In comparison with the existing configuration, the new design shows a better performance, with a 22% reduction of the maximum stress in the bolt member.

Author Contributions: Conceptualization, T.-T.T., S.K. and D.L.; methodology, T.-T.T. and S.K.; software, T.-T.T.; validation, D.L.; formal analysis, T.-T.T.; investigation, D.L.; data curation, T.-T.T. and D.L.; writing—original draft preparation, T.-T.T.; writing—review and editing, T.-T.T. and D.L. All authors have read and agreed to the published version of the manuscript.

Funding: This research was supported by the National Research Foundation of Korea (NRF) grant funded by the Korean government (Ministry of Science and ICT) (No. 2021R1F1A1046912) and by the Human Resources Development of the Korea Institute of Energy Technology Evaluation and Planning(KETEP) grant funded by the Korean government (Ministry of Trade, Industry and Energy) (No. 20214000000180).

Data Availability Statement: The data presented in this study are available on request from the corresponding author.

Conflicts of Interest: The authors declare no conflict of interest.

Appendix A

A formula for calculating the equivalent tensile force.

Under the axial force and moment, the stress distribution σ_s in the tower shell is given:

$$\sigma_s = \frac{M_{ed}}{W_s} - \frac{N_{ed}}{A_s} \quad (A1)$$

in which

$$A_s = \frac{\pi}{4}(D_o^2 - D_i^2); W_s = \frac{\pi}{32} \frac{(D_o^4 - D_i^4)}{D_o} \quad (\text{A2})$$

The tension force F_s in a single segment is the stress distribution σ_s multiplied by the segment area $A_{seg} = A_s/n_b$, and it is given as follows:

$$F_s = \left(\frac{M_{ed}}{W_s} - \frac{N_{ed}}{A_s} \right) A_{seg} \quad (\text{A3})$$

Inserting Equations (A2) into Equation (A3), we obtain:

$$F_s = \frac{1}{n_b} \left(\frac{8M_{ed}D_o}{D_o^2 + D_i^2} - N_{ed} \right) \quad (\text{A4})$$

References

1. CWIF Wind Turbine Accident and Incident Compilation. Available online: <https://docs.wind-watch.org/fullaccidents.pdf> (accessed on 20 November 2022).
2. Shokrieh, M.M.; Rafiee, R. Simulation of Fatigue Failure in A Full Composite Wind Turbine Blade. *Compos. Struct.* **2006**, *74*, 332–342. <https://doi.org/10.1016/J.COMPSTRUCT.2005.04.027>.
3. Lee, K.S.; Bang, H.J. A Study on the Prediction of Lateral Buckling Load for Wind Turbine Tower Structures. *Int. J. Precis. Eng. Manuf.* **2012**, *13*, 1829–1836. <https://doi.org/10.1007/S12541-012-0240-Y>.
4. Chou, J.S.; Tu, W.T. Failure Analysis and Risk Management of a Collapsed Large Wind Turbine Tower. *Eng. Fail. Anal.* **2011**, *18*, 295–313. <https://doi.org/10.1016/J.ENGFAILANAL.2010.09.008>.
5. Tran, T.T.; Lee, D. Development of jacket substructure systems supporting 3MW offshore wind turbine for deep water sites in South Korea. *Int. J. Nav. Archit. Ocean Eng.* **2022**, *14*, 100451. <https://doi.org/10.1016/J.IJNAOE.2022.100451>.
6. Campione, G.; Cannella, F.; Zizzo, M.; Pauletta, M. Buckling Strength of Steel Tube for Lifting Telescopic Wind Steel Tower. *Eng. Fail. Anal.* **2021**, *121*, 105153. <https://doi.org/10.1016/J.ENGFAILANAL.2020.105153>.
7. Ma, Y.; Martinez-Vazquez, P.; Baniotopoulos, C. Buckling analysis for wind turbine tower design: Thrust load versus compression load based on energy method. *Energies* **2020**, *13*, 5302. <https://doi.org/10.3390/en13205302>.
8. Chen, X.; Li, C.; Tang, J. Structural Integrity of Wind Turbines Impacted by Tropical Cyclones: A Case Study from China. *J. Phys. Conf. Ser.* **2016**, *753*, 042003. <https://doi.org/10.1088/1742-6596/753/4/042003>.
9. Alonso-Martinez, M.; Adam, J.M.; Alvarez-Rabanal, F.P.; del Coz Díaz, J.J. Wind Turbine Tower Collapse due to Flange Failure: FEM and DOE Analyses. *Eng. Fail. Anal.* **2019**, *104*, 932–949. <https://doi.org/10.1016/J.ENGFAILANAL.2019.06.045>.
10. Schaumann, P.; Seidel, M. Failure Analysis of Bolted Steel Flanges. *Struct. Fail. Plast.* **2000**, 507–512. <https://doi.org/10.1016/B978-008043875-7/50211-2>.
11. Seidel, M.; Stang, A.; Wegener, F.; Schierl, C.; Schaumann, P. Full-scale Validation of FE Models for Geometrically Imperfect Flange Connections. *J. Constr. Steel Res.* **2021**, *187*, 106955. <https://doi.org/10.1016/j.jcsr.2021.106955>.
12. Zhao, Z.; Dai, K.; Camara, A.; Bitsuamlak, G.; Sheng, C. Wind Turbine Tower Failure Modes under Seismic and Wind Loads. *J. Perform. Constr. Facil.* **2019**, *33*, 04019015. [https://doi.org/10.1061/\(ASCE\)CF.1943-5509.0001279](https://doi.org/10.1061/(ASCE)CF.1943-5509.0001279).
13. Tran, T.-T.; Lee, D. Ultimate Load Capacity Assessment of the L-Type Flange Connection of An Existing 5 MW Wind Tower. In Proceedings of the Asia-Pacific Forum on Renewable Energy, Jeju, Republic of Korea, 31 October–3 November 2021; p. 146.
14. Petersen, C. Tragfähigkeit Imperfektionsbehafteter Geschraubter Ringflansch-Verbindungen. *Der Stahlbau* **1990**, *59*, 97–104.
15. DNVGL-ST-0126; Support Structures for Wind Turbines. DNV GL: Oslo, Norway, 2018.
16. Tran, T.T.; Kim, E.; Lee, D. Development of a 3-legged Jacket Substructure for Installation in the Southwest Offshore Wind Farm in South Korea. *Ocean Eng.* **2022**, *246*, 110643. <https://doi.org/10.1016/J.OCEANENG.2022.110643>.
17. Tran, T.-T.; Kang, S.; Lee, J.-H.; Lee, D. Directional Bending Performance of 4-Leg Jacket Substructure Supporting a 3MW Offshore Wind Turbine. *Energies* **2021**, *14*, 2725. <https://doi.org/10.3390/EN14092725>.
18. Okorn, I.; Nagode, M.; Klemenc, J.; Oman, S. Analysis of Additional Load and Fatigue Life of Preloaded Bolts in a Flange Joint Considering a Bolt Bending Load. *Metals* **2021**, *11*, 449.
19. Ślęczka, L.; Leń, D. Prying Action in Bolted Circular Flange Joints: Approach Based on Component Method. *Eng. Struct.* **2021**, *228*, 111528. <https://doi.org/10.1016/J.ENGSTRUCT.2020.111528>.
20. Petersen, C. *Stahlbau: Grundlagen der Berechnung und baulichen Ausbildung von Stahlbauten*. Springer: Berlin/Heidelberg, Germany, 2012.
21. Seidel, M. *Zur Bemessung Geschraubter Ringflanschverbindungen Von Windenergieanlagen*; Leibniz Universität Hannover: Hannover, Germany, 2001.
22. Tobinaga, I.; Ishihara, T. A Study of Action Point Correction Factor for L-Type Flanges of Wind Turbine Towers. *Wind Energy* **2018**, *21*, 801–806. <https://doi.org/10.1002/we.2193>.
23. DNVGL-RP-C208; Determination of Structural Capacity by Non-Linear Finite Element Analysis Methods. DNV: Oslo, Norway, 2013.

24. Deutscher Ausschuss für Stahlbau DAST-Richtlinie 021: Schraubenverbindungen Aus Feuerverzinkten Garnituren M39 bis M72. 2013.
25. EN 1993-1-8; Eurocode 3: Design of Steel Structures—Part 1-8: Design of Joints. European Union: Brussel, Belgium, 2005.
26. Seidel, M.; Schaumann, P. Measuring Fatigue Loads of Bolts in Ring Flange Connections. In Proceedings of the European Wind Energy Conference, Copenhagen, Denmark, 2–6 July 2001.
27. Tran, T.-T.; Lee, D. Understanding the behavior of I-type flange joint in wind turbine towers: Proposed mechanisms. *Eng. Fail. Anal.* **2022**, *142*, 106750.
28. DNVGL RP-C203; Fatigue Design of Offshore Steel Structures. DNV: Oslo, Norway, 2016.
29. Thage, K.J. Investigation of Flange Connection Capacity for Offshore Wind Turbine Foundations. Doctoral Dissertation, Technical University of Denmark, Lyngby, Denmark, 2017.